Appl. Phys. A (2017) 123:742
DOI 10.1007/s00339-017-1359-6

Applied Physics A
Materials Science & Processing

Thermoplastic deformation of ferromagnetic CoFe-based bulk metallic glasses

Chenguang Wu[1,2,3] · Renchao Hu[1,2] · Qikui Man[1,2] · Chuntao Chang[1,2] · Xinmin Wang[1,2]

Received: 25 June 2017 / Accepted: 27 October 2017

Abstract The superplastic deformation behavior of the ferromagnetic $Co_{31}Fe_{31}Nb_8B_{30}$ bulk metallic glass (BMG) in the supercooled liquid region was investigated. At a given temperature, the BMG exhibits a Newtonian behavior at low strain rates but a non-Newtonian behavior at high strain rates. The high thermal stability of this glassy alloy system offers an enough processing window to thermoplastic forming (TPF), and the strong processing ability was examined by simple micro-replication experiments. It is demonstrated that the TPF formability on length scales ranging down to nanometers can be achieved in the selected experimental condition. Based on the analysis of deformation behavior, the nearly full density sample (i.e. nearly 100%), was produced from water-atomized glassy powders and consolidated by the hot-pressing technique. The sample exhibits good soft-magnetic and mechanical properties, i.e., low coercive force of 0.43 Oe, high initial permeability of 4100 and high Vickers hardness 1398. These results suggest that the hot-pressing process opens up possibilities for the commercial exploitation of BMGs in engineering applications.

✉ Qikui Man
manqk@nimte.ac.cn

[1] Key Laboratory of Magnetic Materials and Devices, Ningbo Institute of Materials Technology and Engineering, Chinese Academy of Sciences, No. 1219 Zhongguan West Road, Zhenhai District, Ningbo 315201, Zhejiang, China

[2] Zhejiang Province Key Laboratory of Magnetic Materials and Application Technology, Ningbo Institute of Materials Technology and Engineering, Chinese Academy of Sciences, Ningbo 315201, Zhejiang, China

[3] Nano Science and Technology Institute, University of Science and Technology of China, Suzhou 215123, Jiangsu, China

1 Introduction

Over the last two decades, bulk metallic glasses (BMGs) have been developed in a wide range of alloys [1]. The amorphous structure of BMGs leads to superhigh strength, large elastic strain limit, and excellent wear and corrosion resistances, typically surpassing those of conventional crystalline metals [2]. In addition, the BMGs with high thermal stability can be thermoplastically processed in the supercooled liquid region (SCLR), where the BMG exists as a highly viscous liquid. As a new class of materials, BMGs are considered unique because they exhibit high strength and can be processed like plastics by thermoplastic forming (TPF) method [3]. Features, such as homogeneous and isotropic structure down to the atomic scale, free residual stresses and relatively small shrinkage, make BMG an ideal candidate for small-scale applications.

Strong TPF ability of BMGs requires low viscosity and long processing time whilst avoiding crystallization in the SCLR. It is typically quantified by the width of SCLR (ΔT_x), i.e. the region bounded between glass transition temperature (T_g) and crystallization temperature (T_x). At present, most studies of TPF focus on Pt-[4], Pb-[5], Zr-[6], Au-[7] and Ce-based [8] BMGs which all present wide SCLR, but the T_g and strength σ_f is relatively low. In contrast, low-cost Fe- and Co-based BMGs exhibit higher T_g and strength σ_f, for example, Fe-based BMGs demonstrated a high thermal stability due to wide supercooled liquid region ΔT_x (exceeding 50 K) and a high T_g (exceeding 870 K), and FeB-based BMGs usually have a wider ΔT_x and a higher T_g [9, 10]. Co-based BMG keeps the fracture strength record among bulk crystalline or glassy alloys, which present better durability and higher working temperature for engineering application [11, 12]. In addition, ferromagnetic BMGs parts with micro-/nanometer dots or wires can be expected to produce

Published online: 08 November 2017

highly functional magnetic devices, such as potential candidate for information storage [13], magnetic domain wall logic devices [14], domain wall diodes [15] and oscillators [16]. Also, the powder metallurgy process can easily make the glassy powders to large samples with nearly full relative density in the SCLR, which can overcome the limitation of BMG dimensions and is free to form a complex shape [17]. However, most ferromagnetic BMGs are difficult to be plastically formed into complex shapes in SCLR because of their rather high viscosity, low thermal stability and glass forming ability (GFA) necessary for TPF process, which limits their practical applications, and very few Fe- or Co-based BMGs exhibit the combination of thermal stability and glass forming ability (GFA) necessary for TPF [18].

FeCoNbB alloys had been extensively studied before 1990s, such as the crystallization behavior of its amorphous ribbons, the magnetic properties of nanocrystalline CoFeNbB alloys and the self-diffusion of alloys [19–21]. In this letter, we studied the superplastic deformation of $Co_{31}Fe_{31}Nb_8B_{30}$ bulk metallic glass, using $Co_{31}Fe_{31}Nb_8B_{30}$ glassy alloy powders prepared by water-atomization method, the high processing ability in SCRL was demonstrated by simple micro-replication experiments, we then fabricated BMGs specimens by hot-pressing technique. This paper reports in detail on the formation, mechanical properties, and magnetic characteristics of the CoFe-based BMG powder compact.

2 Experimental procedure

Alloy ingots with nominal composition $Co_{31}Fe_{31}Nb_8B_{30}$ were made by alloying high-purity elements in an arc furnace under an argon atmosphere. Metallic glassy alloy powders were then prepared by a water-atomization system. Glassy structure was examined by X-ray diffraction with Cu $K\alpha$ radiation. Thermal stability associated with T_g, T_x and ΔT_x was examined by differential scanning calorimetry (DSC). Mechanical properties (σ_f) and TPF experiments were conducted on glassy rods with a diameter of 2 mm using a UTM 5105 testing machine. Vickers hardness (H_v) was measured with a hardness tester under a load of 9.8 N. Magnetic properties of saturation magnetization (I_s), coercive force (H_c), and permeability (μ) were measured with a vibrating sample magnetometer (VSM) under an applied field of 400 kA/m, a B–H loop tracer under a field of 400 A/m and an impedance analyzer under a field of 1 A/m, respectively.

3 Results and discussion

The amorphous structure of the as-cast alloy was identified by X-ray diffraction (XRD) and transmission electron microscopy (TEM). Figure 1a shows the XRD pattern of the $Co_{31}Fe_{31}Nb_8B_{30}$ glassy alloy rod with diameter of 2 mm. Only a broad peak without any crystalline peaks can be seen in the XRD pattern indicating the formation of a glassy phase. Meanwhile, the high-resolution transmission electron microscopy (HRTEM) image of $Fe_{31}Co_{31}Ni_8B_{30}$ glassy alloy rod and corresponding selected area electron diffraction (SAED) pattern are shown in Fig. 1b. No crystalline phase appears in the HRTEM, and the SAED pattern consists of a single diffraction halo without sharp diffraction rings.

As shown in Fig. 2, upon heating, the DSC curve exhibits its distinct endothermic events characteristic of the glass transition, and one-stage exothermic event characteristic of crystallization. It is seen that T_g is 897 K and ΔT_x is 101 K for this alloy. The high thermal stability of this alloy offers a wide enough processing time window for the TPF process.

Figure 3 shows the $Co_{31}Fe_{31}Nb_8B_{30}$ stress–strain curves at temperature of 923 K (T_g+26 K) for strain rate in the range of 1×10^{-4} s^{-1} to 5×10^{-2} s^{-1}. The sample exhibits a peak stress value of almost 3000 MPa at the strain rate of 5×10^{-2} s^{-1} before finally decreasing to 1610 MPa (i.e., flow stress). Such mechanical behavior is called stress overshoot [22]. This phenomenon disappears completely as the strain rate decreases to 2×10^{-3} s^{-1}. The inset photo in Fig. 3 shows the starting sample with a diameter of 2 mm and height of 4 mm and the same sample compressed to a

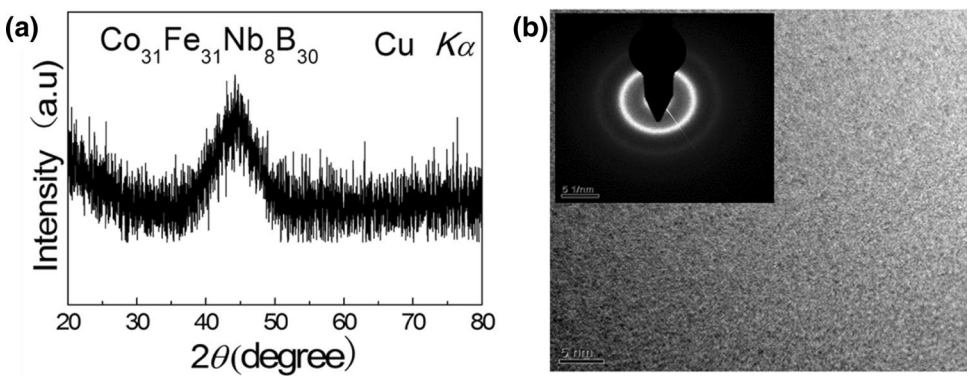

Fig. 1 **a** XRD patterns of the $Fe_{31}Co_{31}Ni_8B_{30}$ cylindrical glassy rods with diameter of 2 mm. **b** HRTEM image of the $Fe_{31}Co_{31}Ni_8B_{30}$ glassy alloy rod. The inset is the related SAED pattern

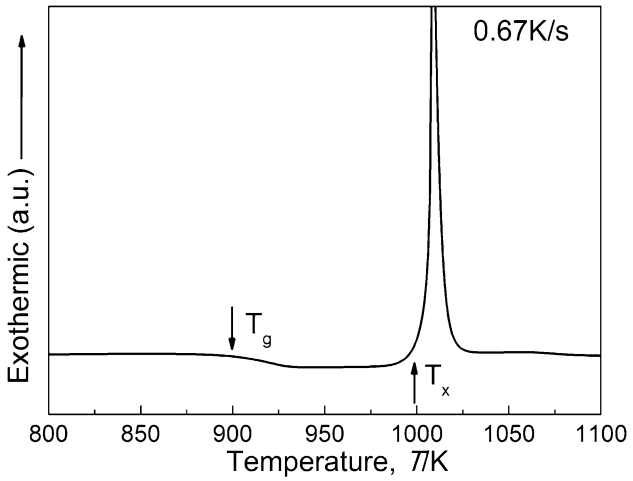

Fig. 2 DSC curves of $Co_{31}Fe_{31}Nb_8B_{30}$ BMG. The inset figure shows XRD patterns of cylindrical glassy rods with diameter of 2 mm

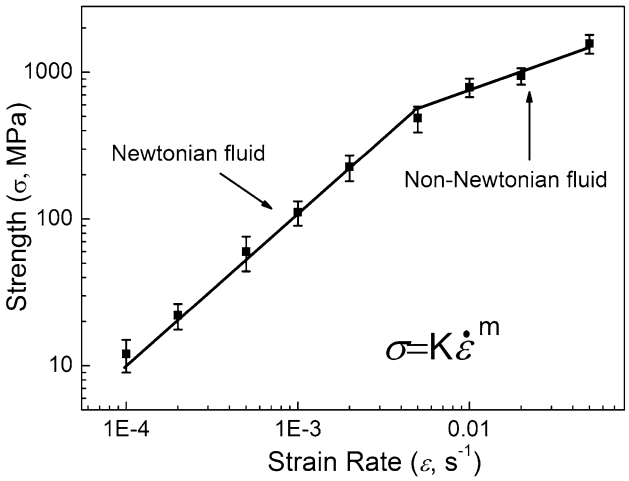

Fig. 4 Strain-rate dependence of strength for $Co_{31}Fe_{31}Nb_8B_{30}$ BMG at 923 K

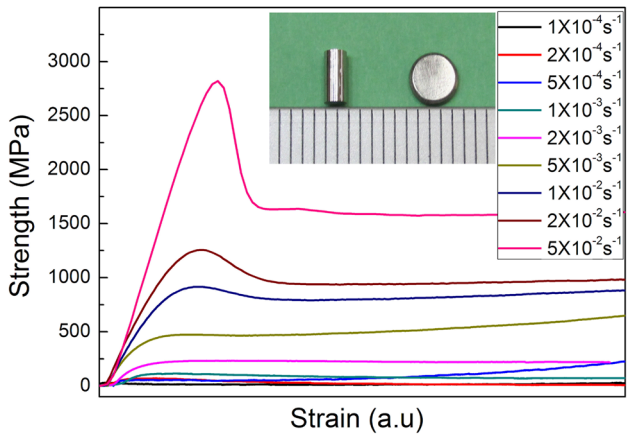

Fig. 3 Stress–strain curves with various strain rates at 923 K of $Co_{31}Fe_{31}Nb_8B_{30}$ BMG. The inset figure shows photographs of the starting sample and the final sample compressed at strain rate 5×10^{-4} s^{-1}

height of 0.5 mm at 923 K. No cracks can be seen, demonstrating good deformability of $Co_{31}Fe_{31}Nb_8B_{30}$ in SCLR. To further study the flow behavior of the BMG, we investigated the relationship between flow stress and strain rate using the following equation: $\sigma flow = K\dot{\varepsilon}^m$, where σflow is the flow stress, K is a constant, $\dot{\varepsilon}$ is the strain rate and m is the strain rate sensitivity exponent [23]. According to the equation and the data from Fig. 3, we calculated different values of m for $Co_{31}Fe_{31}Nb_8B_{30}$ metallic glass in Fig. 4. It is found that the m value of $Co_{31}Fe_{31}Nb_8B_{30}$ is approximately equal to 1 in the strain rate range of 1×10^{-4} s^{-1} to 5×10^{-3} s^{-1}, indicating that the deformation behavior of the BMG is Newtonian flow, which means the strain rate is proportional to the stress directly [22]. However, as the strain rate increased from 1×10^{-2} s^{-1} to 5×10^{-2} s^{-1}, m is about 0.5, the deformation behavior exhibits a non-linear response to stress, i.e., non-Newtonian flow [22]. The change in the deformation behavior from Newtonian to non-Newtonian flow should be closely related to free volume [24]. At high strain rate, the free volume will be rapidly increased and prior to take place in where stress is concentrated, which results in stress overshoot and deformation of BMG far from the ideal Newtonian flow [15]. In general, no stress overshoot phenomenon appears at temperature of 923 K (T_g+26 K) for strain rate in the range of 1×10^{-4} s^{-1} to 2×10^{-3} s^{-1}, indicating that the BMG in this case has an ideal and infinite plasticity.

To demonstrate the flow workability of this BMG system in the SCLR, simple micro-replication experiments were done at 953 K under a pressure of 30 MPa for 60 s. For prevention of oxidation, all samples and molds were wrapped up together with copper foil. As shown in Fig. 5a, the $Co_{31}Fe_{31}Nb_8B_{30}$ BMG sheet with 1 mm thickness is hot-embossed into a coin. It can be seen clearly that the embossed pattern is integrated without any obvious disfigurement. And a diamond-shape pattern on length scales ranging down to micrometers was successfully replicated on the BMG sheet, even the scratches on the original mold are clearly reproduced, as shown in Fig. 5b. To further examine the Nano-imprinting ability of this BMG, the Al_2O_3 particles with diameters about 80 nm were placed on this BMG sheet for TPF process. After ultrasonic cleaning, many Nano-dots were successfully replicated into this BMG sheet, and several residue particles also can be seen on the surface as shown in Fig. 5c. All final parts remain fully amorphous as verified by X-ray diffraction shown in Fig. 5d. These results demonstrate the good TPF formability of the CoFe-based BMG in the selected experimental condition. The good TPF formability attributed to their rather low viscosity, high

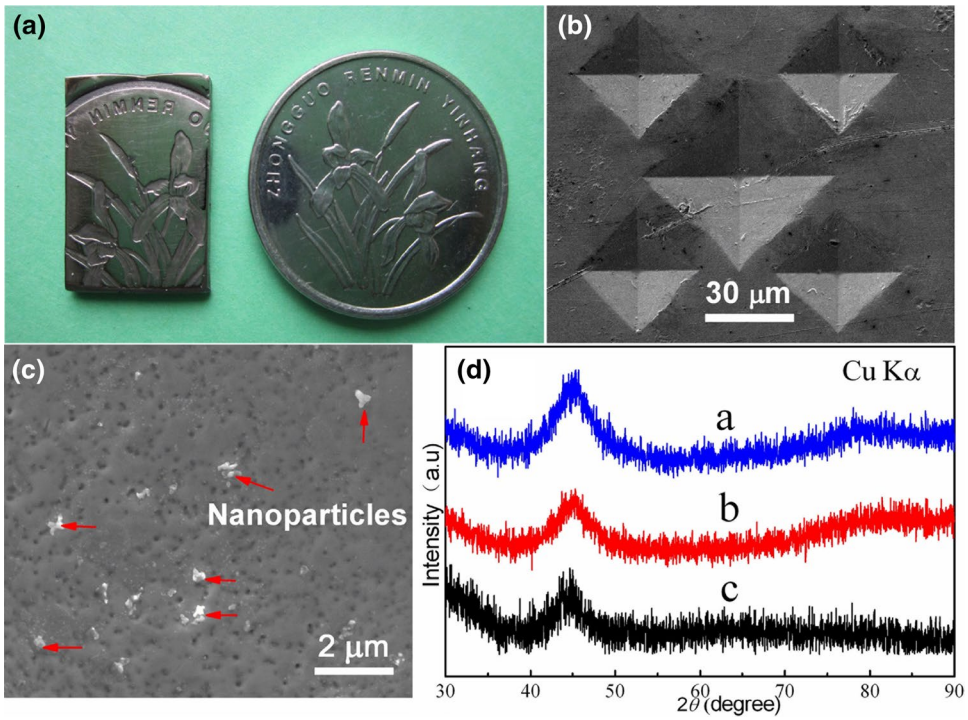

Fig. 5 **a** The reticular pattern imprinted onto the $Co_{31}Fe_{31}Nb_8B_{30}$ BMG sheet at 953 K under a pressure of 30 MPa for 60 s. **b** The diamond-shape pattern replicated on the BMG sheet. **c** Nano-dots were replicated into BMG sheet: place the Al_2O_3 particles with diameters about 80 nm on BMG sheet, increase temperature to 953 K and apply 30 MPa pressure for 60 s, SEM micrograph was observed after ultrasonic cleaning. **d** XRD patterns of final samples after TPF process

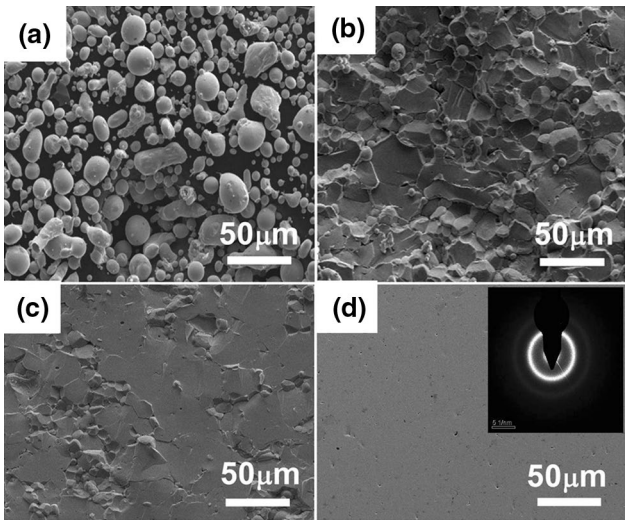

Fig. 6 **a** SEM micrograph of the $Co_{31}Fe_{31}Nb_8B_{30}$ powder fabricated by water-atomization method. **b** Cross-section of $Co_{31}Fe_{31}Nb_8B_{30}$ BMG at 923 K under a pressure of 84 MPa. **c** Cross-section under a pressure of 112 MPa. **d** Polished surface for cross-section of sample, the inset is the related SAED pattern

thermal stability, the homogeneous structure, free residual stress and small shrinkage of the CoFe-based BMG [4]. Thus, they are expected to be the favorable materials for nano-forming or nano-imprinting.

Figure 6a shows the SEM image of the $Co_{31}Fe_{31}Nb_8B_{30}$ water-atomized powders in a size range of 38–74 μm. The cross-sections of $Co_{31}Fe_{31}Nb_8B_{30}$ BMG compacts at 923 K under pressure of 84 and 112 MPa are shown in Fig. 6b, c, respectively. It can be found that the spacing among the powders is large at lower hot-pressing, and both sides of the interface come into physical contact. Figure 6b shows that the powders started to merge with each other under 84 MPa, indicating an increase in sintering kinetics and solid state diffusion bonding. And with the pressure increased gradually, the distance between the powder is getting smaller and smaller. Meanwhile, the bonding method from the physical bond transformed into a metallurgical bond gradually. With further hot-pressing at 112 MPa, the fracture surface becomes smoother and less undulating. The relative density of this powder compact reaches a high value of 99%. As shown in Fig. 6d, the polished surfaces of sample hot-pressed at 112 MPa exhibit smooth outer surface and metallic luster, and the SAED pattern consists of a single diffraction halo without sharp diffraction rings. This indicates that bulk $Co_{31}Fe_{31}Nb_8B_{30}$ powder compact with highly dense structure has been prepared successfully. Thermoplastic bonding process can be explained by the following mechanisms [25]. In general, oxidation occurs on the surface of amorphous powder, in which shaping is significantly less than the internal metal. In the process of compression, oxide layer under the action of lateral tensile failure forms a hollow, and the hole is filled with the pristine power with pressure, caused both sides of the interface change to metallic bond forms from physical contact, and pristine continuous oxide film was broke and scattered in BMG. The mechanical properties of the powder compact have been also investigated. The sample exhibits good wear resistance, maximum

friction coefficient of 0.736, and wear rate at room temperature of about 1.32×10^{-6} mm^{-3}/ (N·m). The Vickers hardness value is 1398 with an applied load of 9.8 N.

Figure 7 shows the hysteresis loop of the bulk powder compact sample fabricated under pressure of 112 MPa. The magnetic core cut from the disk sample exhibits high initial permeability ($\mu_{max}=4100$) and low value of coercivity (H_c=0.43 Oe). The good soft-magnetic properties in conjunction with a wide-range SCLR make possible to convert powders into the bulk form easily by powder metallurgy technique, so specimens with a large size and complex shape can be simply achieved. In summary, the combination of TPF ability and good mechanical properties make this ferromagnetic BMGs promising candidates for applications as structural and functional materials.

4 Conclusions

1. The superplastic deformation behavior of the ferromagnetic $Co_{31}Fe_{31}Nb_8B_{30}$ bulk metallic glass (BMG) in the supercooled liquid region was investigated.
2. At 923 K, the BMG exhibits a Newtonian behavior at low strain rates (1×10^{-4} s^{-1} to 5×10^{-3} s^{-1}) but a non-Newtonian behavior at high strain rates (1×10^{-2} s^{-1} to 5×10^{-2} s^{-1}). No stress overshoot phenomenon appears indicating that the BMG has an ideal and infinite plasticity in that case.
3. Nearly full density sample in the SCLR can overcome the limitation of BMGs dimensions and is free to form a complex shape.
4. This CoFe-based BMG with high initial permeability ($\mu_{max}=4100$), low value of coercivity ($H_c=0.43$ Oe), and high fractures strength (σ_f) of approximately 5000 MPa at room temperature is promising for future applications as a new functional material.

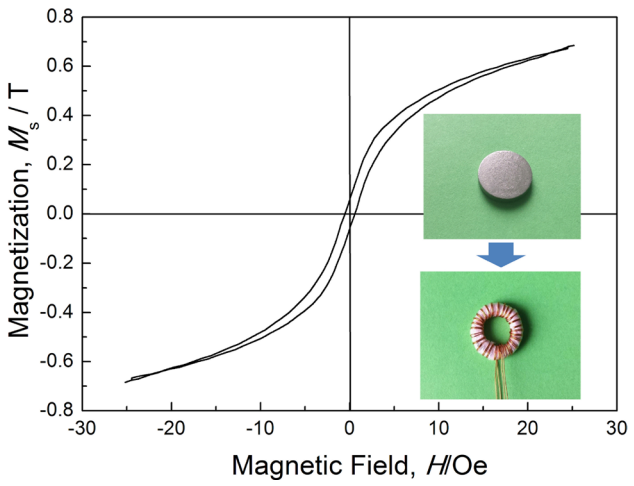

Fig. 7 B–H loops for ring-shaped $Co_{31}Fe_{31}Nb_8B_{30}$ BMG sample fabricated from powder by hot-pressing process at 923 k under a pressure of 112 MPa

Acknowledgements This work was supported by the National Natural Science Foundation of China (Grant No. 51301189), Zhejiang Province Public Technology Research and Industrial Projects (Grant No. 2015C31043).

References

1. A. Inoue, N. Nishiyama, New bulk metallic glasses for applications as magnetic-sensing, chemical, and structural materials. MRS Bull. **32**(8), 651–658 (2011)
2. A.L. Greer, M. Glasses, Science **267**(5206), 1947–1953 (1995)
3. J. Qiang, D. Estevez, C. Chang, Q. Man, R.-W. Li, X. Wang, A. Inoue, High strength CoFe-based glassy alloy with high thermal stability. Mater. Lett. **114**, 126–128 (2014)
4. G. Kumar, H.X. Tang, J. Schroers, Nanomoulding with amorphous metals. Nature **457**(7231), 868–872 (2009)
5. Y. Saotome, K. Itoh, T. Zhang, A. Inoue, Superplastic nanoforming of Pd-based amorphous alloy. Scripta Mater. **44**(8–9), 1541–1545 (2001)
6. J. Schroers, T.M. Hodges, G. Kumar, H. Raman, A.J. Barnes, Q. Pham, T.A. Waniuk, Thermoplastic blow molding of metals. Mater. Today **14**(1–2), 14–19 (2011)
7. J. Schroers, T. Nguyen, S. O'Keeffe, A. Desai, Thermoplastic forming of bulk metallic glass—applications for MEMS and microstructure fabrication. Mater. Sci. Eng. A 449–451, 898–902 (2007)
8. B. Zhang, D.Q. Zhao, M.X. Pan, W.H. Wang, A.L. Greer, Amorphous metallic plastic. Phys. Rev. Lett. **94**(20), 205502, (2005)
9. S.F. Guo, Z.Y. Wu, L. Liu, Preparation and magnetic properties of FeCoHfMoBY bulk metallic glasses. J. Alloys Compd. 468(1–2), 54–57 (2009)
10. S.F. Guo, J.L. Qiu, P. Yu, S.H. Xie, W. Chen, Fe-based bulk metallic glasses: Brittle or ductile?. Appl. Phys. Lett. **105**(16), 161901 (2014)
11. J. Wang, R. Li, N. Hua, T. Zhang, Co-based ternary bulk metallic glasses with ultrahigh strength and plasticity. J. Mater. Res. **26**(16), 2072–2079 (2011)
12. A. Inoue, B. Shen, H. Koshiba, H. Kato, A.R. Yavari, Cobalt-based bulk glassy alloy with ultrahigh strength and soft magnetic properties. Nat. Mater. **2**(10), 661–663 (2003)
13. S. Sun, C.B. Murray, D. Weller, L. Folks, A. Moser, Monodisperse FePt nanoparticles and ferromagnetic FePt nanocrystal superlattices. Science 287(5460), 1989–1992 (2000)
14. D.A. Allwood, G. Xiong, C.C. Faulkner, D. Atkinson, D. Petit, R.P. Cowburn, Magnetic domain-wall logic. Science 309(5741), 1688–1692 (2005)
15. D.A. Allwood, G. Xiong, R.P. Cowburn, Domain wall diodes in ferromagnetic planar nanowires. Appl. Phys. Lett. **85**(14), 2848–2850, (2004)
16. G. Finocchio, N. Maugeri, L. Torres, B. Azzerboni, Domain wall dynamics driven by a localized injection of a spin-polarized current. Magnet. IEEE Trans. **46**(6), 1523–1526 (2010)
17. G. Xie, D.V. Louzguine-Luzgin, H. Kimura, A. Inoue, Nearly full density $Ni_{52.5}Nb_{10}Zr_{15}Ti_{15}Pt_{7.5}$ bulk metallic glass obtained by spark plasma sintering of gas atomized powders. Appl. Phys. Lett. **90**(24), 241902 (2007)

18. W. Zhang, C. Fang, Y. Li, Ferromagnetic Fe-based bulk metallic glasses with high thermoplastic formability. Scripta Mater. **69**(1), 77–80 (2013)
19. I.L. Kraus, V. Haslar, P. Duhaj, P. Svec, V. Studnicka, The structure and magnetic properties of nanocrystalline Co21Fe64—xNbxB15 alloys. Mater. Sci. Eng. A 226–228, 626–663 (1997)
20. V. Soyka, L. Kraus, Magnetic properties of stress/field annealed nanocrystalline FeCoNbB alloys. J. Magnet. Magnet. Mater. **203**(1–3), 220–222 (1999)
21. F. Faupel, P.W. Huppe, K. Ratzke, Pressure dependence and isotope effect of self-diffusion in a metallic glass. Phys. Rev. Lett. **65**(10), 1219–1222 (1990)
22. J. Lu, G. Ravichandran, W.L. Johnson, Deformation behavior of the $Zr_{41.2}Ti_{13.8}Cu_{12.5}Ni_{10}Be_{22.5}$ bulk metallic glass over a wide range of strain-rates and temperatures. Acta Mater. **51**(12), 3429–3443 (2003)
23. W.J. Kim, D.S. Ma, H.G. Jeong, Superplastic flow in a $Zr_{65}Al_{10}Ni_{10}Cu_{15}$ metallic glass crystallized during deformation in a supercooled liquid region. Scripta Mater. **49**(11), 1067–1073 (2003)
24. K.C. Chan, L. Liu, J.F. Wang, Superplastic deformation of $Zr_{55}Cu_{30}Al_{10}Ni_5$ bulk metallic glass in the supercooled liquid region. J. Non-Cryst. Solids **353**(32–40), 3758–3763 (2007)
25. W. Chen, Z. Liu, J. Schroers, Joining of bulk metallic glasses in air. Acta Mater. **62**, 49–57 (2014)